Research Article

COMPARISON OF DUAL THREE-PHASE AND SIX-PHASE SURFACE MOUNTED PERMANENT MAGNET MOTOR FOR TRACTION DRIVE APPLICATIONS

Duong Le Doan QUY[1], *Duc Quang NGUYEN*[2], *Phi Do CHI*[3], *Tuan Nghia LUONG*[4], *Vuong Dang QUOC*[1,*]

[1]School of Electrical and Electronic Engineering, Hanoi University of Science and Technology, Viet Nam
[2]Faculty of Electrical Engineering, Electric Power University, Ha Noi, Vietnam
[3]Electrical-Electronic Engineering, Cao Thang Technical College, Ho Chi Minh, Viet Nam
[4]Faculty of Automotive Engineering, Van Lang School of Technology, Van Lang University, Ho Chi Minh City, Vietnam

duong.dlq212493@sis.hust.edu.vn, dinh.buiminh@hust.edu.vn, quangndhtd@epu.edu.vn, dochiphi@caothang.edu.vn, nghia.lt@vlu.edu.vn

[*]Corresponding author: Vuong Dang Quoc; vuong.dangquoc@hust.edu.vn

DOI: 10.15598/aeee.v24ix.250602

Article history: Received Jun 5, 2025; Revised Jul 17, 2025; Accepted Aug 5, 2025; First Published Aug 25, 2025.

Abstract. *Permanent magnet synchronous motors (PMSMs) are widely used in industrial and commercial applications such as electric vehicles, robotics, and aerospace, owing to their high power and torque density, operational stability, and exceptional efficiency. The integration of permanent magnets (PMs) eliminates the need for an external excitation current, thereby minimizing excitation losses. Recently, six-phase motor systems have emerged as viable alternatives to traditional three-phase configurations, offering enhanced fault tolerance and improved control performance under fault conditions. Critical research areas for PMSMs in electric vehicle applications include the design and implementation of advanced control strategies to achieve high precision, reliability, and energy efficiency. This study proposes a comparative electromagnetic performance analysis of dual three-phase and six-phase surface-mounted permanent magnet motors, utilizing both analytical and finite element methods. To further optimize the proposed motors, a segmented skewing technique is applied, demonstrating additional improvements in performance characteristics. This research contributes to a deeper understanding of these motor configurations for traction drive applications.*

Keywords

Surface-mounted permanent magnet synchronous motor, outer rotor configuration, back EMF, electromagnetic torque, cogging torque, skewed permanent magnet.

1. Introduction

Climate change has emerged as a pressing global issue, driven by both natural processes and intensified human activities. One of its most apparent consequences is global warming, primarily caused by the extensive emissions generated daily by industrial operations and internal combustion engines (ICEs). In response to this, reducing emissions from transportation systems has become a central objective in the pursuit of sustainable technologies. Electric motors, recognized for their high efficiency, precise control, and superior reliability, offer a compelling alternative to traditional ICEs, thereby playing a vital role in the global shift toward environmentally friendly mobility solutions.

Among various electric motor technologies, Permanent Magnet Synchronous Motors (PMSMs) have gained widespread adoption across numerous industrial sectors, including electric vehicles, robotics, and

aerospace [1–3]. This prevalence is attributed to their compact size, high efficiency, reliability, and structural flexibility, along with their high power and torque density, operational stability, and exceptional efficiency. Their performance is further enhanced by the use of rare-earth permanent magnets (PMs), such as neodymium-iron-boron (NdFeB) and samarium-cobalt (SmCo), which eliminate the need for traditional DC excitation systems, effectively minimizing excitation losses [4, 5]. PMSMs are extensively deployed in a wide range of low-speed and high-torque applications, including medical devices, hybrid and electric vehicles, marine propulsion systems, hoisting mechanisms, mining operations, and oil and gas exploration. PMSMs can be classified based on magnet placement and rotor topology into surface-mounted (SPM) and interior (IPM) types, as well as inner-rotor and outer-rotor configurations. In recent years, outer-rotor Surface-Mounted Permanent Magnet Synchronous Motors (SPMSMs) have attracted significant interest due to their suitability for compact, torque-demanding machinery. Studies have demonstrated that outer-rotor SPM designs can achieve up to 40% lower copper losses and approximately 8.5% higher torque compared to inner-rotor equivalents of the same magnet size [6]. These improvements are attributed to the larger available space for pole placement and the torque advantage arising from the increased rotor diameter, which directly influences output torque. Furthermore, the development of multiphase motor technology, particularly six-phase PMSMs, represents a pivotal advancement in electric machine design. These systems have emerged as viable alternatives to traditional three-phase configurations [7, 8]. By distributing the electrical load across more phases, six-phase configurations offer enhanced fault tolerance, improved thermal performance, and greater overload capacity compared to conventional three-phase systems. These features make them ideal for high-reliability applications such as marine propulsion, aerospace systems, and other mission-critical environments. In terms of winding strategies, fractional-slot concentrated winding (FSCW) has become a preferred choice in high-torque, low-speed applications due to its compact coil structure, reduced copper losses, short end-windings, and improved efficiency [9–12]. However, FSCW designs typically exhibit lower winding factors and higher harmonic content compared to integral-slot windings, presenting challenges in terms of magnetic performance and thermal management, particularly in outer-rotor motor architectures [13]. Thus, careful selection of pole and slot combinations remains essential in optimizing performance for targeted applications.

Control strategies for six-phase PMSMs have also become a prominent area of research [14]. These systems are typically categorized into symmetrical six-phase, asymmetrical six-phase, and dual three-phase configurations. While asymmetrical six-phase systems are known to produce lower torque ripple when operated using six-step inverters, modern high-frequency pulse-width modulation (PWM) techniques allow symmetrical six-phase machines to achieve comparable torque quality, making both symmetrical and dual three-phase topologies viable alternatives for high-performance drive systems.

In this study, a comparative electromagnetic performance analysis of dual three-phase and six-phase SPMSMs is proposed. This analysis utilizes both analytical methods and the finite element method (FEM). An analytical model is developed to calculate the necessary dimensional parameters of two proposed motors at the same power rate of 130 kW, powered by a dual three-phase system and a symmetrical independent six-phase system, respectively (Figure 1). Subsequently, FEM is conducted to compute and analyze the electromagnetic characteristics based on these analytical calculations. To further optimize the selected motor configuration, a segmented skewing technique is applied, demonstrating additional improvements in performance characteristics. This research aims to contribute to a deeper understanding of these motor configurations for traction drive applications.

Section 2 presents the analytical design methodology for SPMSMs with both inner and outer rotor configurations, detailing the step-by-step design process for each topology. In Section 3, three-dimensional finite element method (3D-FEM) simulations are performed to evaluate and compare the electromagnetic characteristics of the two motor structures. Section 4 provides a comprehensive summary of the performance metrics obtained from both configurations. Future work will focus on multi-physics analyses, whose results are expected to offer valuable insights for selecting the most suitable inner rotor (IR) or outer rotor (OR) configurations for high-speed SPMSM applications.

2. Background of Analytical Design

In this part, the analytical design of a SPMSM with OR configuration is presented. The inner diameter (D_{ir}) of the rotor is defined via the maximum magnet stress (σ_m), i.e.,

$$D_{ir} = \left(\frac{2.M}{\sigma_m.\pi}\right)^{\frac{1}{3}}, \tag{1}$$

where M is the electromagnetic torque (N.m). The air-gap flux density generated by the PMs plays a crucial role in determining the back electromotive force (EMF) and the torque quality produced by the SPMSM. In this research, Neodymium (NdFeB) magnets of grade N38SH are selected due to their high magnetic performance and thermal stability.

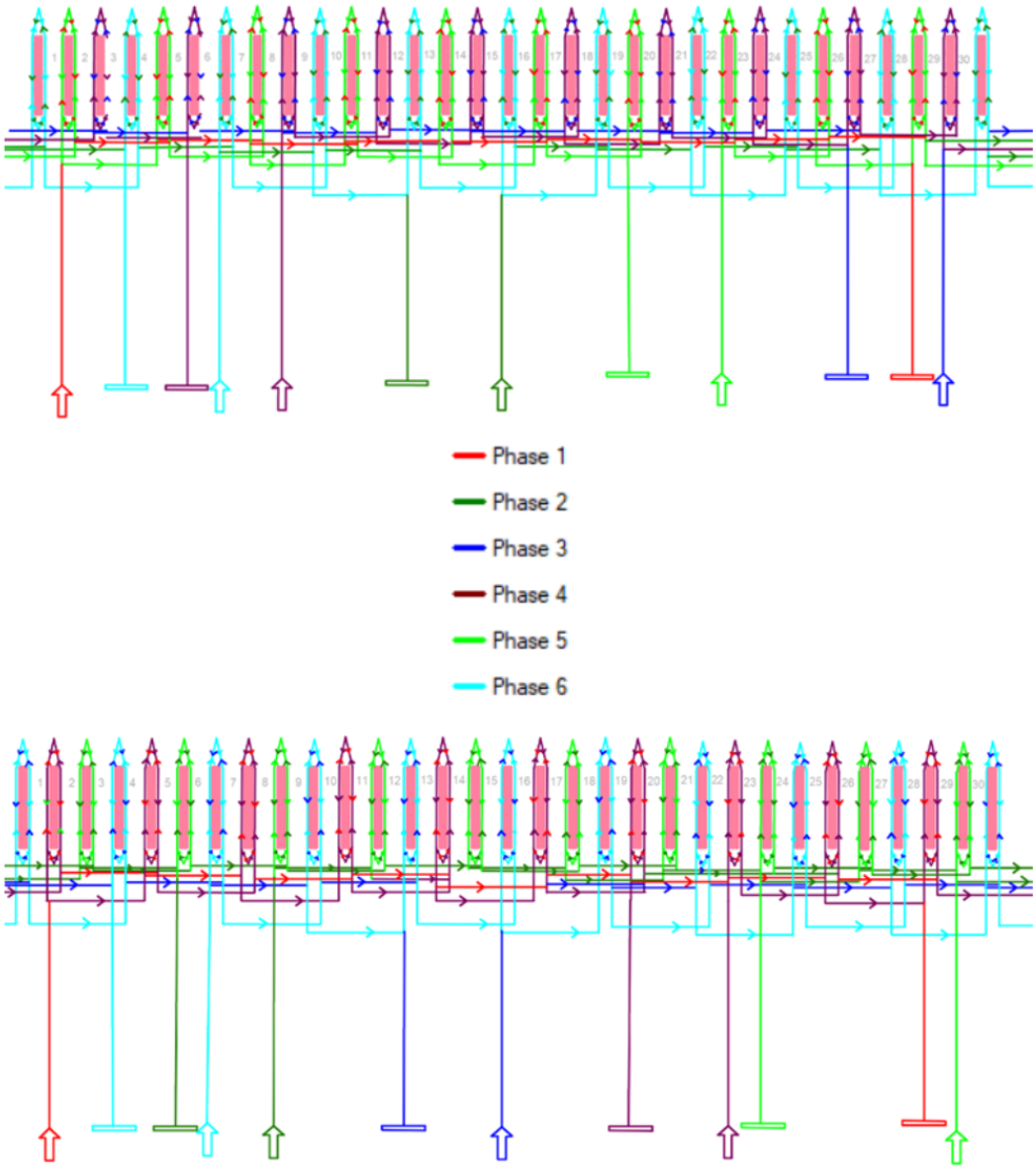

Fig. 1: The winding diagram of SPMSM: Dual three-phase system (top); Six-phase system (bottom).

The magnetic flux density in the air gap between stator and rotor can be defined as [4]:

$$B_g = \frac{4}{\pi} \cdot \sin\left(\frac{\rho_{pm}}{2}\right) \cdot B_m, \tag{2}$$

where B_m is the magnetic flux density of the PM and ρ_{pm} is the electric angle of the PM.

The magnet thickness is determined based on [4]:

$$d_m = \frac{\mu_r \cdot g_{eff} \cdot B_g \cdot \pi}{B_r \cdot 4 \cdot \sin\left(\frac{\rho_{pm}}{2}\right) - B_g \cdot \pi} \tag{3}$$

where B_r is the remenant PM, μ_r is the relative permeability of PM, and g_{eff} is the effective length of air gap. The width of the PM is determined by [17].

$$W_m = 2a \cdot \frac{L_p}{\pi} \tag{4}$$

It should be noted that the magnet length (L_p) is selected to be equal to the rotor length. The magnetic flux of the PM is then determined by:

$$\phi_m = B_m \cdot W_m \cdot L_p. \tag{5}$$

The length of stator yoke (h_{sy}) is defined as

$$h_{sy} = \frac{B_m \cdot W_m}{2 \cdot B_s}. \tag{6}$$

The magnetic flux on the tooth (ϕ_t) is defined as:

$$\phi_t = \frac{\phi_m \cdot 2 \cdot p}{Q_s}. \tag{7}$$

The width of tooth (w_t) is determined by:

$$W_t = \frac{\phi_t}{B_t \cdot k_j \cdot L_s}, \tag{8}$$

where B_t is the magnetic flux density on the tooth, k_j is the pressed factor of the stator yoke, and Q_s is the number of slots. The slot bottom width (b_{s1}) is defined as:

$$b_{s1} = \pi \times \frac{D_{os} - 2(h_{so} + h_w)}{Q_s} - w_t, \tag{9}$$

where h_{so} and h_w are respectively slot opening and wedge height. The slot top width (b_{s2}) is determined as:

$$b_{s2} = \sqrt{\frac{b_{s1}^2 - 4\pi \times A_{slot}}{Q_s}}, \tag{10}$$

where A_{slot} is the slot area. The slot height (h_s) is defined as:

$$h_s = \frac{2 \cdot A_{slot}}{b_{s1} + b_{s2}}. \tag{11}$$

Finally, the number of turns is determined as follows:

$$N = \frac{U_s}{2\sqrt{2}\pi \cdot f \cdot q \cdot k_w \cdot B_g \cdot \cos\left(\frac{20\pi}{180}\right) \cdot D_{is} \cdot L} \tag{12}$$

where q the number of slot per pole per phase, k_w the winding factor and U_s is the line voltage $\left(U_s = \frac{U_{DC}}{\sqrt{2}}\right)$. It should be noted that for the two different phase distribution cases, there will be different phase voltage equations as follows:

+ Case 1: Dual three-phase system:

$$U_n = \frac{U_s}{\sqrt{3}} \tag{13}$$

+ Case 2: Independent six-phase system:

$$U_n = \frac{U_s}{2} \tag{14}$$

where U_n is the motor phase voltage calculated according to the above 2 cases. Based on the initial parameters of the proposed motor given in Table 1, the main dimensional parameters of the OR SPMSM after using the above analytical equations are give in Table 2.

3. Results and discussion

In this section, the FEM is applied to simulate the electromagnetic parameters of the proposed motor. The main dimensions of this motor are given in Table 1 and 2. Figure 1 shows the winding arrangement of the SPMSM in a dual three-phase system and independent six-phase system. The distribution of magnetic flux density is shown in Figure 2.

Tab. 1: Required parmeters of SPMSM with OR configuration.

Parameters	Value	Unit
Rate Power	130	kW
DC Bus Voltage	650	V
Number of phases	6	pha
Number of slots	30	slots
Number of pole pairs	5	pole
Rate torque	960	Nm

It is observed that the maximum magnetic flux densities for the dual three-phase and independent six-phase systems are 1.959 T and 2.059 T, respectively, measured at the same tooth edge location, resulting in a difference of 0.1 T. The higher value of 2.059 T in the independent six-phase system is relatively close to the saturation limit, increasing the risk of magnetic saturation under fault conditions. Therefore, the dual three-phase system, with its lower flux density, provides a safer operating margin, thereby enhancing the motor's reliability and overall operational stability. Figure 3 presents the torque waveforms for both systems. It is evident that the torque output of the independent six-phase system is smoother and more stable. The cogging torque distribution caused by the interaction between the rotor's PMs and the stator teeth is shown in Figure 4. It can be observed that the dual three-phase system exhibits higher cogging torque compared to the independent six-phase system. Furthermore, the torque ripple of the independent six-phase system is significantly lower, reaching only 35.73%, while the dual three-phase system exhibits a much higher ripple of 61.78% nearly twice as much. At the same output power, the efficiency of the independent six-phase system is 0.352% lower than that of the dual three-phase system. This indicates that motors using the dual three-phase system are more energy-efficient during operation compared to those with the independent six-phase system. Taking into account the torque quality and the advantages and disadvantages of each system, the PMSM with the independent six-phase system is selected for the next stage of the study, which involves implementing magnet skewing by segment.

The back-EMF distribution is shown in Figure 5. The total harmonic distortion (THD) of the back-EMF for the dual three-phase and independent six-phase systems is respectively 50.96% and 41.39%. The air-gap magnetic flux distribution is illustrated in Figure 6. Both systems exhibit sinusoidal waveforms. However, the dual three-phase system has a higher amplitude, resulting in greater torque production compared to the independent six-phase system. Finally, simulation

Tab. 2: Required parmeters of SPMSM with dual three-phase and six-phase system.

Parameter	Dual three-phase system	Six-phase system	Unit
Stator outer diameter	289	289	mm
Rotor outer diameter	348.65	343.37	mm
Shaft diameter	172.95	178.44	mm
Rotor length	420	420	mm
Tooth width	13.52	10.84	mm
Slot height	29.7	29.6	mm
Magnet thickness	4.5	4.5	mm
Magnet electrical angle	138	126	Degree
Number of turns	4	4	Turn
Conductor diameter	1.004	1.103	mm

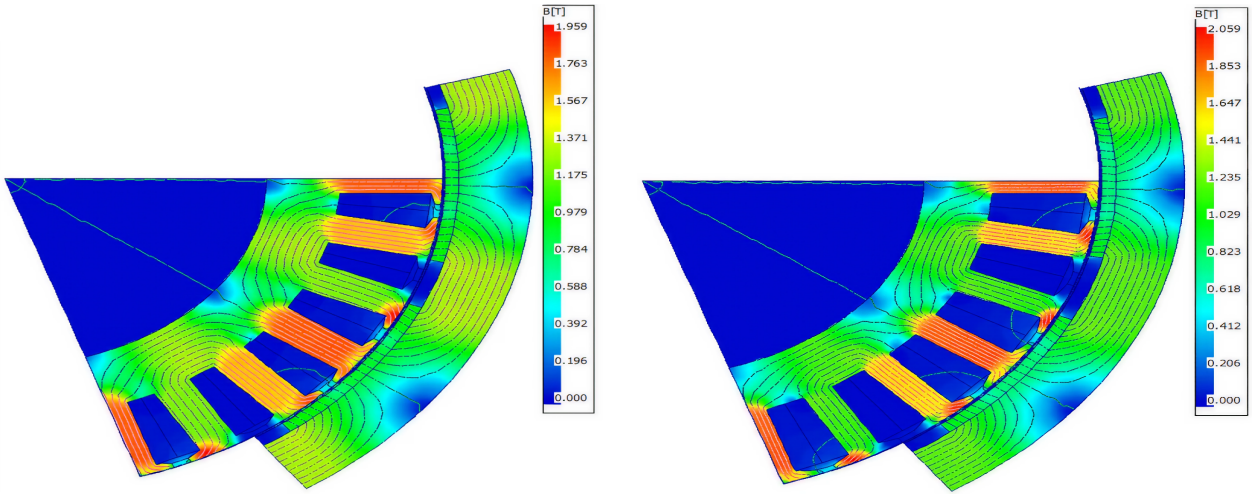

Fig. 2: Magnetic flux density distribution: Dual three-phase system (top); Six-phase system (bottom).

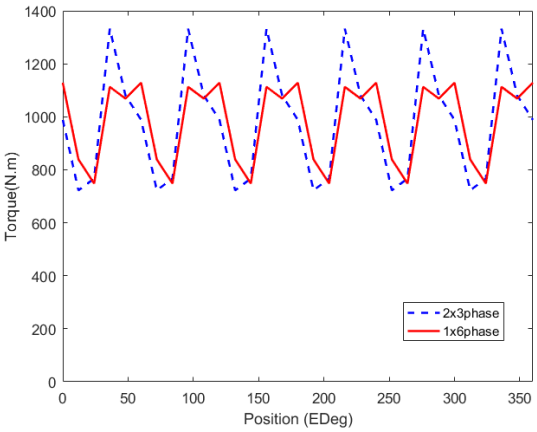

Fig. 3: Waveform of output torques with dual three-phase and six-phase systems.

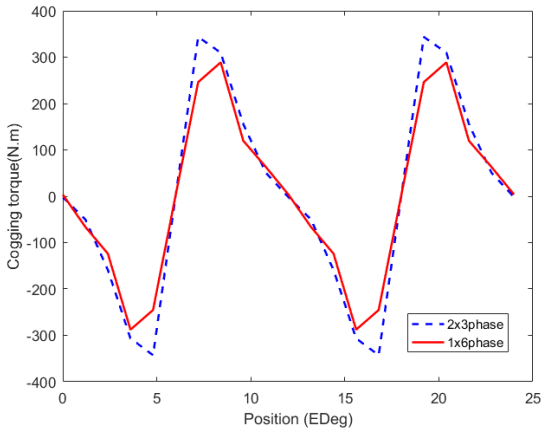

Fig. 4: Waveform of cogging torques with dual three-phase and six-phase systems.

results with dual three-phase and six-phase systems are given in Table 3.

It can be seen that the motor with a dual three-phase system exhibits higher efficiency than the one with an independent six-phase system. The motor configured with a dual three-phase system exhibits higher efficiency compared to the motor using an independent six-phase system. Both motors meet the design requirements, delivering an output power of 130 kW and an output torque of 960 Nm. The dual three-phase system achieves an efficiency of 95.016%, whereas

Tab. 3: Simulation results with dual three-phase and six-phase systems.

Parameter	Dual three-phase system	Six-phase system	Unit
Ouput power	130470	130370	W
Efficiency	95.016	94.664	%
Torque Ripple	61.782	35.73	%
Power factor	0.97354	0.95033	
Shaft torque	963.55	962.83	N.m
Back EMF THD	50.96	41.39	%

Tab. 4: Simulation results with before and after skewed PMs.

Parameter	Before skewing	After skewing	Unit
Ouput power	130370	130990	W
Efficiency	94.664	94.493	%
Torque Ripple	35.73	8.9876	%
Power factor	0.95033	0.94557	
Shaft torque	962.83	967.38	N.m
Back EMF THD	41.39	27.69	%

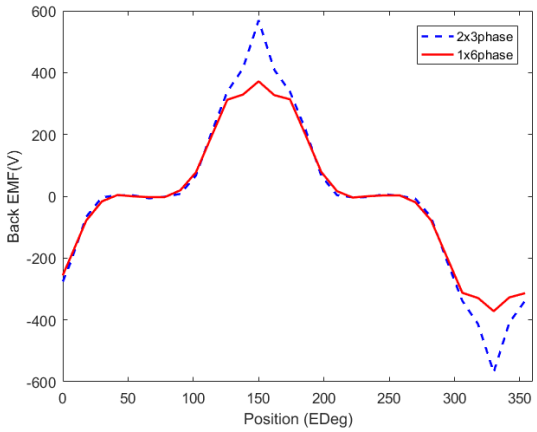

Fig. 5: Waveform of back EMF with dual three-phase and six-phase systems.

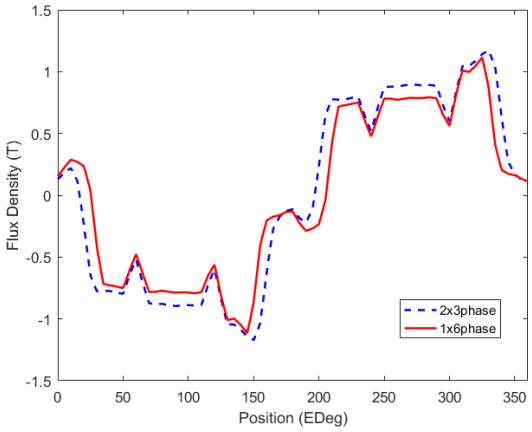

Fig. 6: Magnetic flux density distribution at the air gap with dual three-phase and six-phase systems.

the independent six-phase configuration reaches only 94.664%. This represents an efficiency improvement of 0.352% in favor of the dual three-phase system. This difference becomes significant when multiple motors operate simultaneously, contributing to notable energy savings. The power factor values for the two configurations are 0.97 for the dual three-phase system and 0.95 for the independent six-phase system, indicating that the dual three-phase system utilizes active power more effectively.

4. Skewing Technique for PMs

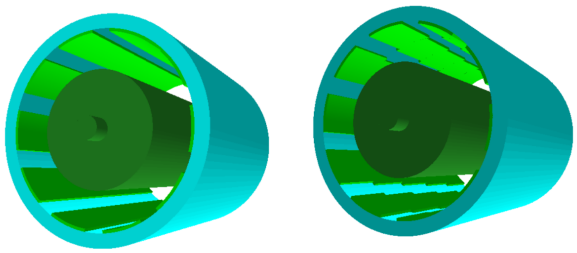

Fig. 7: 3D-modeling of the outer rotor configuration with before skewed PMs (left) and after skewed PMs (right).

Based on the results of the SPMSM outer rotor given in Table 3, the FEM is applied to calculate and simulate the electromagnetic parameters of the motor with an independent six-phase control system under two conditions: without magnet skewing and with magnet skewing. Figure 7 illustrates the 3D models of both the non-skewed and skewed rotor configurations. In this study, the magnet skewing technique is implemented by dividing each magnet into five segments, each segment having different skew angles. These skew angles, which are symmetrical with respect to 0° were given

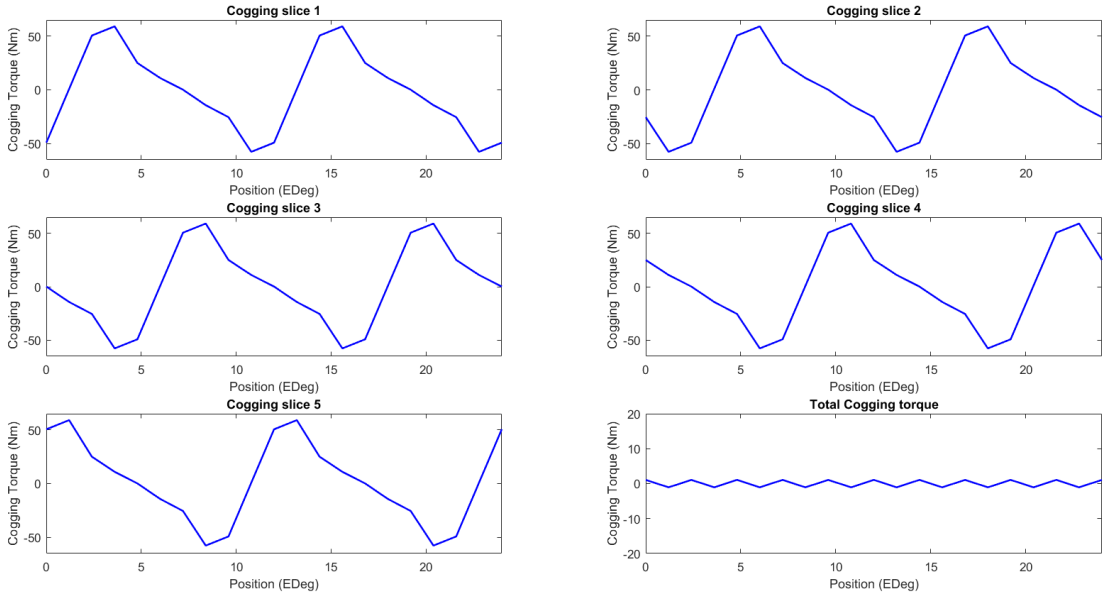

Fig. 8: Waveform of cogging torques in each slice after using the skew PMs.

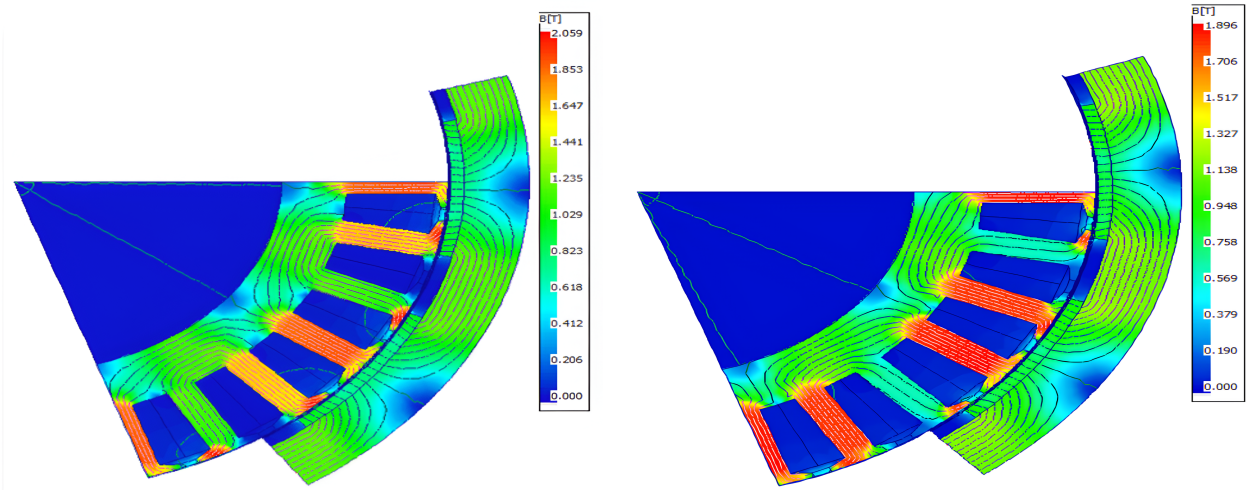

Fig. 9: Flux density distribution on the stator and rotor before skewing (top) and after skewing (bottom).

in [4, 5]. The principle behind the reduction of torque ripple using the magnet skewing technique is explained as follows. The cogging torque waveforms generated by each magnet segment after applying the skewing method are illustrated in Figure 8.

It is evident that each magnet generates a cogging torque waveform with a distinct phase shift within one electrical cycle, which is determined by its skewing angle. When these individual cogging torque components are superimposed, they partially cancel each other, resulting in a smoother net output torque. By selecting an optimal skewing angle, cogging torque can be almost entirely suppressed. However, this method inherently reduces the average torque due to the attenuation of higher-order harmonic components. Furthermore, as the skewing angle increases, torque ripple diminishes, but this improvement is accompanied by a decline in average torque [16]. To maintain the desired output power and preserve the nominal average torque, the stator current provided by the motor controller must be appropriately adjusted [17]. The magnetic flux density distributions for both scenarios are depicted in Figure 9. Without magnet skewing, the peak flux density reaches 2.059 T, whereas with skewing, the maximum value decreases to 1.896 T. This reduction demonstrates that magnet skewing effectively mitigates the risk of magnetic saturation under fault conditions.

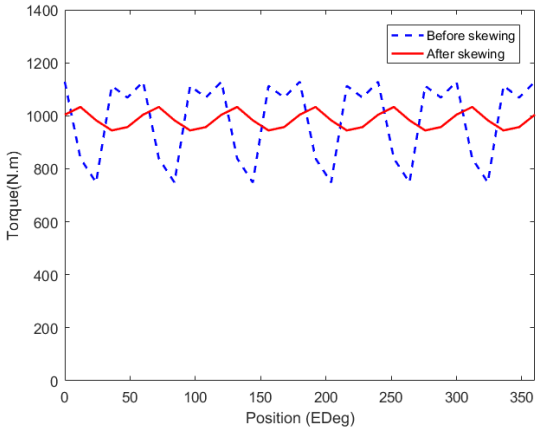

Fig. 10: Waveform of output torques with before and after skewed PMs.

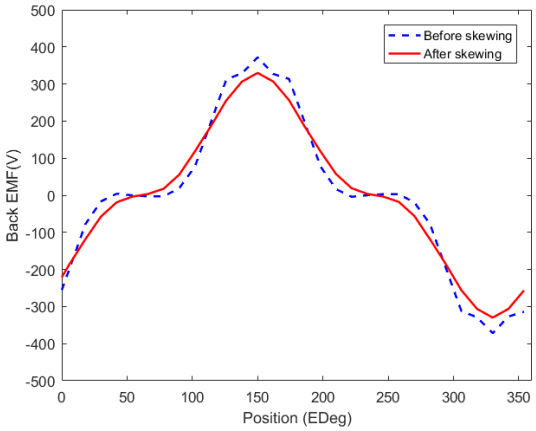

Fig. 12: Waveform of back EMFs with before and after skewed PMs.

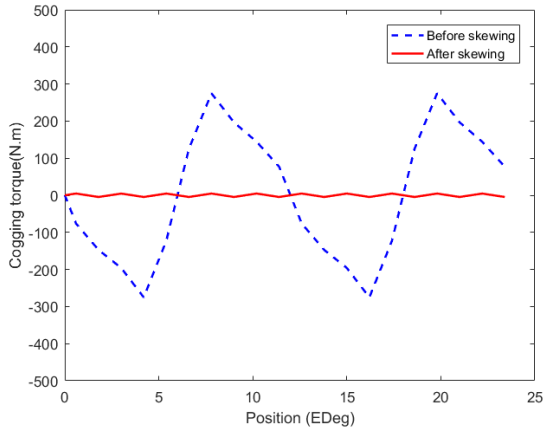

Fig. 11: Waveform of cogging torques with before and after skewed PMs.

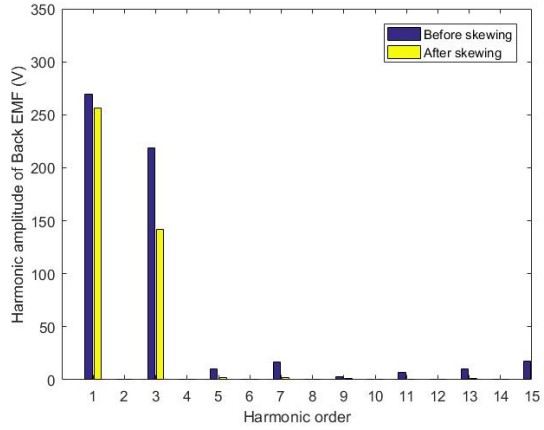

Fig. 13: Harmonic components of back EMF with before and after skewed PMs.

Figure 10 presents the output torque waveforms for both cases. Before applying magnet skewing, the torque waveform exhibits substantial oscillations with an average torque of 984.2547 Nm. The significant reduction in cogging torque is shown in Figure 11. This results are in a much smoother torque output. Furthermore, the torque ripple reduces significantly from 35.73% down to 8.9876%, clearly demonstrating the effectiveness of the magnet skewing technique in enhancing the torque quality of the motor.

The waveform of back EMFs after doing skewed PMs is presented in Figure 12. It shoud be noted that after skewing, the total THD of the back EMF decreases from 41.39% to 27.69%, marking a 13.7% improvement as shown in Figure 13. The magnetic flux density distribution across the air gap is shown in Figure 14. It can be observed that the flux distribution before and after magnet skewing remains nearly unchanged. The key performance parameters of the motor under both conditions are summarized in Table 4. These results

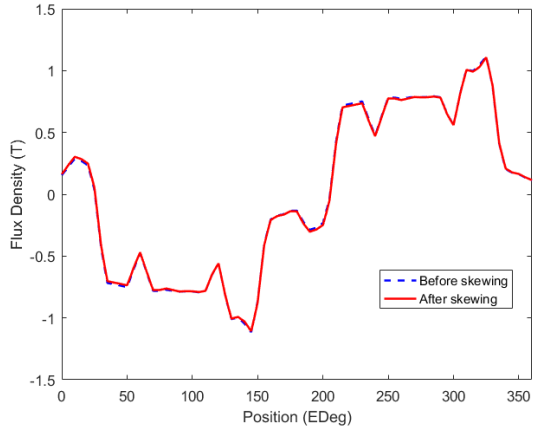

Fig. 14: Temperature Magneic flux density distribution at the air gap with before and after skewed PMs.

align with expectations and validate the effectiveness of the proposed magnet skewing technique in this study.

5. Conclusion

This paper presented the analytical design of two 130 kW SPMSMs with a 650 V DC bus, employing dual three-phase and independent six-phase configurations. Comparative analysis revealed that the independent six-phase system excels in torque quality, stability, and electromagnetic performance, while the dual three-phase system achieves higher efficiency. The application of magnet skewing further enhanced performance, reducing torque ripple from 35.73% to 8.99% and back-EMF THD from 41.39% to 27.69%, confirming the effectiveness of both the analytical design approach and skewing technique.

In the future work, it will focus on applying and developing advanced motor design methodologies using optimization techniques such as particle swarm optimization, genetic algorithms, and other approaches. The target objectives will include improving torque characteristics, reducing cogging torque and torque ripple, and minimizing material cost.

Author Contributions

D. L. D. Q. and V. D. Q. developed the analytical model and finite elemment method for the conventional and Hairpin winding configurations of V-Shaped IPMSM. D. B. M. and T. N. L. performed the simulation of the proposed motor. Q. N. D. and P. D. C. checked and analysed results of the manuscript. All authors contributed to the final version of the manuscript.

References

[1] HAIFENG, Z., D. ZHI, Z. JINGHUA. Optimization design and analysis of permanent magnet synchronous motor based on VC. *20th International Conference on Electrical Machines and Systems (ICEMS), Sydney, NSW, Australia.* 2017, pp. 1-4. DOI: 10.1109/ICEMS.2017.8055957.

[2] LEE, J. H., et al. Particle Swarm Optimization Algorithm With Intelligent Particle Number Control for Optimal Design of Electric Machines. *IEEE Transactions on Industrial Electronics.* 2018, vol. 65, no. 2, pp. 1791-1798. DOI: 10.1109/TIE.2017.2760838.

[3] JIN, F., et al. Analysis of a Six-Phase Direct-Drive Permanent Magnet Synchronous Motor with Novel Toroidal Windings. *IEEE Vehicle Power and Propulsion Conference (VPPC), Hanoi, Vietnam.* 2019, pp. 1-6. DOI: 10.1109/VPPC46532.2019.8952311.

[4] TRUONG, T. C., et al. Optimal Electromagnetic Parameters of SPMSM for Electric Vehicles Based on Genetic Algorithm Technique. *International Journal on Electrical Engineering and Informatics.* 2024, vol. 16, no. 1, pp. 137–148. DOI: 10.15676/ijeei.2024.16.1.9.

[5] GAO, Y., et al. Neural Network aided PMSM multi-objective design and optimization for more-electric aircraft applications. *Chinese Journal of Aeronautics.* 2022, vol. 35, iss. 10, pp. 233–246. DOI: 10.1016/j.cja.2021.08.006.

[6] TAHA, H. M., I. ALNAAB. Designs of PMSMs with Inner and Outer Rotors for Electric Bicycle Applications. *Kurdistan Journal of Applied Research.* 2019, vol. 4, no. 1, pp. 20–25. DOI: 10.24017/science.2019.1.4.

[7] PATEL, V. I., J. WANG, W. WANG, X. CHEN. Six-Phase Fractional-Slot-per-Pole-per-Phase Permanent-Magnet Machines With Low Space Harmonics for Electric Vehicle Application. *IEEE Transactions on Industry Applications.* 2014, vol. 50, no. 4, pp. 2554-2563. DOI: 10.1109/TIA.2014.2301871.

[8] SCUILLER, F., E. SEMAIL, J.-F. CHARPENTIER, P. LETELLIER. Multi-criteria-based design approach of multi-phase permanent magnet low-speed synchronous machines. *IET Electric Power Applications.* 2009, vol. 3, no. 2. DOI: 10.1049/iet-epa:20080003.

[9] PLUTA, W. A. Core loss models in electrical steel sheets with different orientation. *Czestochowa University of Technology.* 2011.

[10] PONOMAREV, P. Tooth-Coil Permanent Magnet Synchronous Machine Design for Special Applications. *Acta Universitatis Lappeenrantaensis.* 2013.

[11] SEO, U.-J., et al. General Characteristic of Fractional Slot Double Layer Concentrated Winding Synchronous Machine. *Journal of Electrical Engineering and Technology.* 2013, vol. 8, iss. 2, pp. 282–287. DOI: 10.5370/JEET.2013.8.2.282.

[12] JUSSILA, H., P. SALMINEN, M. NIEMELA, J. PYRHONEN. Guidelines for Designing Concentrated Winding Fractional Slot Permanent Magnet Machines. *International Conference on Power Engineering, Energy and Electrical Drives, Setubal, Portugal.* 2007, pp. 191-194. DOI: 10.1109/POWERENG.2007.4380186.

[13] ISLAM, M. Z., S. S. R. BONTHU, S. CHOI. Comparison of two different winding topologies for external-rotor five-phase PM-assisted synchronous reluctance motor in vehicle applications. *IEEE International Electric Machines and Drives Conference (IEMDC), Miami, FL, USA.* 2017, pp. 1-6. DOI: 10.1109/IEMDC.2017.8002399.

[14] CHE, H. S., W. P. HEW. Dual three-phase operation of single neutral symmetrical six-phase machine for improved performance. *IECON 2015 - 41st Annual Conference of the IEEE Industrial Electronics Society, Yokohama, Japan*. 2015, pp. 001176-001181. DOI: 10.1109/IECON.2015.7392259.

[15] CHI, D. D., H. B. HUU, B. D. THANH, V. D. QUOC. A Novel Skewed Permanent Magnet Technique for Improving Performances of SPMSMs with Outer Rotor Type. *Tenth International Conference on Communications and Electronics (ICCE), Danang, Vietnam*. 2024, pp. 643-647. DOI: 10.1109/ICCE62051.2024.10634690.

[16] FENG, L., et al. Study on performance of low-speed high-torque permanent magnet synchronous motor with dynamic eccentricity rotor. *Energy Reports*. 2022, vol. 8, pp. 1421–1428. DOI: 10.1016/j.egyr.2022.03.018.

[17] LI, D., R. QU, J. LI, W. XU. Consequent-Pole Toroidal-Winding Outer-Rotor Vernier Permanent-Magnet Machines. *IEEE Transactions on Industry Applications*. 2015, vol. 51, no. 6, pp. 4470-4481. DOI: 10.1109/TIA.2015.2458953.